HHS Public Access

Author manuscript

Neuron. Author manuscript; available in PMC 2017 August 17.

Published in final edited form as:

Neuron. 2016 August 17; 91(4): 748–762. doi:10.1016/j.neuron.2016.07.024.

Regrowth of serotonin axons in the adult mouse brain following injury

Yunju Jin[1,*], **Sarah E. Dougherty**[1,*], **Kevin Wood**[2], **Landy Sun**[1], **Robert H. Cudmore**[1], **Aya Abdalla**[2], **Geetha Kannan**[1,3], **Mikhail Pletnikov**[1,3], **Parastoo Hashemi**[2,4], and **David J. Linden**[1,5]

[1]Solomon H. Snyder Department of Neuroscience, The Johns Hopkins University School of Medicine, 725. N. Wolfe Street, Baltimore MD 21205 USA

[2]Department of Chemistry, Wayne State University, 5101 Cass Avenue, Detroit, MI 48202 USA

[3]Department of Psychiatry and Department of Molecular and Comparative Pathobiology, The Johns Hopkins University School of Medicine; Department of Molecular Microbiology and Immunology, Bloomberg School of Public Health, The Johns Hopkins University, 600 N. Wolfe Street, Baltimore MD 21205 USA

Summary

It is widely believed that damaged axons in the adult mammalian brain have little capacity to regrow, thereby impeding functional recovery after injury. Studies using fixed tissue have suggested that serotonin neurons might be a notable exception, but remain inconclusive. We have employed *in vivo* two-photon microscopy to produce time-lapse images of serotonin axons in the neocortex of the adult mouse. Serotonin axons undergo massive retrograde degeneration following amphetamine treatment and subsequent slow recovery of axonal density which is dominated by new growth with little contribution from local sprouting. A stab injury that transects serotonin axons running in the neocortex is followed by local regression of cut serotonin axons and followed by regrowth from cut ends into and across the stab rift zone. Regrowing serotonin axons do not follow the pathways left by degenerated axons. The regrown axons release serotonin and their regrowth is correlated with recovery in behavioral tests.

eTOC blurb

[5]Corresponding author: dlinden@jhmi.edu, 410-614-1529 (voice).

[4]Present Address: Department of Chemistry and Biochemistry, University of South Carolina, 631 Sumter Street, Columbia, SC 29208 USA

[*]Equal contribution

Author Contributions

Y.J. designed, performed and analyzed the immunohistochemistry, in vivo imaging and behavioral experiments and co-wrote the manuscript. S.E.D. designed and performed immunohistochemical experiments related to the stab injury. K.W. performed a portion of the voltammetry experiments. L.S. and R.H.C. developed analysis tools for in vivo imaging data. A.A. performed a portion of the voltammetry experiments. G.K. assisted with the behavioral experiments and their analysis. M.P. designed and helped to analyze the behavioral experiments. P.H. designed and analyzed the voltammetry experiments. D.J.L. directed the overall experimental design and analysis and co-wrote the manuscript

Jin et al. use in vivo two-photon imaging to reveal serotonin axon regrowth following injury in adult mouse brain. They find that damaged serotonin axons can regrow from their severed ends and that regrown axons are competent to release serotonin.

Introduction

Axons that sustain damage in the adult mammalian brain are thought to fail to regrow and this failure is believed, at least in part, to result from factors in the matrix of tissue that broadly inhibit axonal growth (Chew et al., 2012). Rather, the limited functional rewiring that occurs after brain trauma is proposed to be dominated by the compensatory local sprouting of neighboring uninjured axons (Tuszynski & Steward, 2012). There have been suggestions from studies in both damaged brain (Hawthorne et al., 2011) and damaged, grafted spinal cord (Alilain et al., 2011; Yoo et al., 2013; Kanno et al., 2014) that axons of serotonin neurons might have an atypical capacity for regrowth. Following a lesion of serotonin axons in the rat neocortex with a high dose of amphetamine, there is a gradual reappearance of serotonin-immunoreactive axons over many months (Molliver et al., 1990; Mamounas et al., 2000). While suggestive, these fixed-tissue studies have been inconclusive. They were unable to distinguish degeneration and subsequent regrowth from a transient amphetamine-mediated down-regulation of serotonin levels within intact axons. Nor have these studies been able to distinguish potential regrowth from damaged axons from compensatory sprouting of local undamaged axons. Thus, the regrowth of serotonin axons remains an important topic of debate that speaks to a central view in the recovery of neural function. Here, in order to observe the serotonin axon recovery process directly and disambiguate the results from fixed-tissue studies, we have performed in vivo 2-photon time-lapse imaging over many months in adult serotonin transporter-EGFP BAC transgenic mice (Gong et al., 2003) following several forms of injury.

The serotonin system in the CNS has been broadly implicated in the regulation of affect, aggression, sexual behavior, sleep and cognitive function (Muller and Jacobs, 2010). It originates in the raphe nuclei, a distributed series of cell groups with weakly-defined boundaries flanking the midline of the midbrain and brainstem (Hornung, 2003). The rostral group of raphe nuclei, consisting of the supralemniscal nucleus, median raphe and dorsal raphe, contains serotonin neurons that project widely to forebrain structures including all regions of the neocortex, the striatum, olfactory bulbs, amygdala and hippocampus. In the rodent, the axons of the rostral raphe nuclei are almost entirely thin and unmyelinated (Azmitia and Gannon, 1983; Wilson and Molliver, 1994). Those fibers that innervate the neocortex form a C-shape when observed in the sagittal plane: they pass through the lateral hypothalamus and the basal forebrain, running in the medial forebrain bundle (MFB). The fibers then turn dorsally, elaborating branches that form projections to the frontal cortex, and then turn posteriorly to innervate parietal, temporal and occipital cortices, respectively (Figure 1, upper right panel). Electron microscopy of neocortical serotonin axons shows that the vast majority of vesicle-bearing varicosities in serotonin axons have no corresponding postsynaptic density laden with serotonin receptors. This suggests that the action of serotonin on its targets is mainly produced by slow, diffuse volume transmission rather than

fast, localized synaptic transmission (Hornung, 2003; Beaudet and Descarries, 1978; De Filipe and Jones, 1988).

Results

Immunohistochemical experiments show PCA-induced degeneration and subsequent recovery of serotonin axons

To visualize serotonin neurons we have used a BAC transgenic mouse in which the promoter of the serotonin transporter drives expression of soluble EGFP to produce a cytoplasm-filling marker almost completely restricted to serotonin neurons in the adult brain (Slc6a4-EGFP mouse, Gong et al., 2003) as indicated by EGFP + serotonin double label immunohistochemistry (Figure S1). Initially, we have sought to characterize the effects of amphetamine treatment using immunohistochemical techniques. Mice received 8 intraperitoneal injections over 4 days of either *para*-chloro-amphetamine (PCA; 20 mg/kg), a particularly toxic amphetamine derivative (Fuller, 1992) or saline. After a recovery period ranging from 1 day to 6 months, the mice were sacrificed and sagittal slices near the midline were processed for immunohistochemistry using antibodies against EGFP, to show serotonin neurons, and NeuN, to reveal a subset of neuronal cell bodies. Figure 1 shows exemplar confocal images taken 1 day after PCA treatment, revealing swollen serotonin axons in neocortical regions and the rostral MFB (see also Figure S2 for in vivo imaging of swollen axons 1 day after PCA treatment). There were no swollen axons seen in the more proximal portions of the axonal trajectory including those that pass through the linear nucleus of the raphe, the posterior hypothalamus and the more caudal portions of the MFB (data not shown). This pattern is consistent with the early stages of retrograde axonal degeneration and is congruent with a well-established literature on amphetamine-induced degeneration of serotonin axons in rats, which has gone to great lengths to demonstrate the hallmarks of degeneration including swollen, irregular axons (Molliver et al., 1990) and has used immuno-electron microscopy to show amphetamine-evoked destruction of microtubules and degenerated mitochondria in such axons (Adori et al., 1980). Figure 2 shows representative images taken 1 week after PCA or saline treatment, starting with the serotonergic cell bodies of origin in the dorsal raphe nucleus and continuing with their long C-shaped projection through the MFB and ending in the occipital cortex. These images reveal that PCA treatment produced a significant loss of serotonin axons in all of the cortical regions examined as well as in the rostral aspect of the MFB. Importantly, neither the cell bodies of origin in dorsal raphe (Figures 2A and 2B) nor the initial portion of the axons running in the linear nucleus of the raphe or the posterior hypothalamus were affected by PCA treatment while the caudal portion of the MFB showed a small degree of axonal loss. When the period after PCA treatment was extended to 3 and 6 months, substantial recovery of EGFP immunoreactivity was observed in the MFB and neocortex (Figures 2C and S3).

These findings are consistent with previous reports using amphetamine treatment in rats followed by immunohistochemistry with antibodies directed against serotonin (Molliver et al., 1990; Mamounas et al., 2000; O'Hearn et al., 1988). However, because here the serotonin axons are visualized with an antibody to untethered cytoplasmic EGFP, the present results argues against a model in which intact serotonin axons are merely depleted of

serotonin by PCA treatment and then slowly refill. Could PCA treatment somehow lead to a reduction of EGFP expression driven by the promoter of the serotonin transporter? As one way to address this question, we measured serotonin transporter immunoreactivity in proximal, undegenerated axons coursing through the linear nucleus of the raphe complex, 1 week after saline or PCA treatment. No difference in serotonin transporter immunoreactivity was seen between saline and PCA treatment in these images (saline: 55.8 ± 1.7 % area occupied by serotonin transporter signal; PCA: 60.1 ± 6.7 % area, n = 3/group). By contrast, PCA treatment produced a profound decrease in serotonin transporter immunoreactivity in the same distal locations where EGFP signal was lost such as somatosensory cortex (saline: 32.9 ± 1.4 % area occupied by serotonin transporter signal; PCA: 4.3 ± 0.4 % area, n = 7/group).

As a further test of the possibility that apparent serotonin axons degeneration was merely an artifact of reduced Slc6a4-EGFP expression in intact axons, we injected the virus AAV5-EF1a-DIO-hChR2(H134R)-EYFP-WPRE-pA into the dorsal raphe of serotonin transporter-Cre mice to produce surface membrane labeling (Tsai et al., 2009) of the complete extent of dorsal raphe serotonin neurons, including their axonal projections to the neocortex. Following a one-month period to allow for expression and transport of EYFP, mice received PCA or saline treatment and were then sacrificed one week or three months thereafter. This was followed by triple-label immunohistofluorescence to reveal EYFP and serotonin transporter expression in axons of the frontal and somatosensory cortex as well as NeuN to reveal neuronal nuclei (Figure S4). Because Cre recombinase activity is irreversible, this treatment yields a mouse in which EYFP expression is no longer subject to regulation, being under the control of the strong, ubiquitous EF1a promoter rather than the promoter of the serotonin transporter gene. In layer 1 of somatosensory cortex, in a saline treated mouse sacrificed one week later, 23.7 ± 1.0 % of the area was occupied by serotonin transporter immunoreactivity and 12.3 ± 0.9 of the area was occupied by EYFP immunoreactivity (n=8 mice). Of the EYFP positive pixels, 79.6 ± 3.9 % were also serotonin transporter positive. This indicates that virally-introduced EYFP selectively labeled approximately half of the serotonin transporter-positive axons. Importantly, 1 week after PCA treatment, serotonin transporter immmunoreactivity was reduced to 7.0 ± 0.9 % and EYFP immunoreactivity was reduced to 3.6 ± 0.3 % (n=6). When these measurements were repeated on a cohort of mice allowed to recover for 3 months after PCA treatment, we observed partial recovery in both measures (serotonin transporter: 14.2 ± 1.0 % and EYFP 8.1 ± 0.4%, n=9), similar to the degree of recovery seen using Slc6a4-EGFP mice (Figure 2). These results argue that PCA treatment does indeed cause massive degeneration of serotonin axons rather than merely appearing to do so through an effect on EGFP expression in Slc6a4-EGFP mice.

In vivo time lapse imaging shows that serotonin axon recovery after PCA lesion is dominated by new growth from outside the imaging volume, not local sprouting from surviving axons

To assess the dynamics of axonal regrowth and allow for within-animal comparisons, we employed chronic *in vivo* two-photon microscopy. Here, we define regrowth as growth of axons in response to injury irrespective of the cellular origin of growth (that is, either from damaged or undamaged axons). Cranial windows were implanted overlying the

somatosensory cortex of serotonin transporter-EGFP mice. After an 11-day recovery period, a z-stack encompassing layer 1 was acquired, followed by a second pre-treatment image taken 3 days later. Then, mice were injected with either PCA (n = 9) or saline (n = 4). Imaging of the same region was then continued at weekly intervals for as long as possible, ranging from 13 to 29 weeks. Figure 3A shows exemplar maximal z-stack projections and 3-D axon tracings for PCA and saline treated mice. When total axonal length was calculated for each time point, it was revealed that PCA treatment produced a large decrease measured 1 week after treatment (25.5 ± 3.5% of baseline, mean ± SEM, n = 9) while the saline group was unaffected (98.0 ± 1.6%, n = 4). The PCA-treated group showed a slow, gradual recovery (64 ± 6.2% at t = 19 weeks, n = 4) that can be appreciated in a movie showing 3-D projections and rotations of exemplar analyzed volumes (Movie S1). In contrast, total axonal length of the saline-treated group was highly stable (91.8 ± 4.8 %, t = 19 weeks, n = 3). Similar results were found when the total number of axonal branch points was scored (Figure S5). To further analyze the recovery process, axonal segments were assigned to several groups: Surviving axons, which persisted after treatment, sprouted axons which grew as new branches elaborated from those axons which survived, and new axons which only appeared in the field of view at some point after treatment. Figure 3B shows that the slow recovery of total axonal length following PCA treatment is almost entirely due to the presence of new axons. The rate of local sprouting from surviving axons following PCA is very low (5.2 ± 1.1 % at t = 19 weeks, n = 4) and is comparable to the rate seen in saline-treated control mice (4.3 ± 1.6% at t = 19 weeks, n = 3, Figure 3B). The axons that survive PCA treatment are not merely dying slowly: Of the surviving axons present 1 week after PCA, 96.5% are still present at week 19, slightly more than the 81.7% survival rate of saline-treated axons over this same period.

Most of the new serotonin axons appearing after PCA treatment completely traverse the imaged volume from one weekly time-point to the next. This is consistent with the overall rostrocaudal course of serotonin axons in neocortical layer 1 (Hornung, 2003). However, in some cases, new axons can be observed to gradually extend within the field of view from week-to-week as shown in Figure 4. Sprouting axons can also be seen to gradually extend within the field of view.

Are the new axons that appear in the imaged volume after PCA treatment growing from the shafts or severed ends of damaged axons or are they axons that have sprouted from survivors adjacent to our field of view and that have then grown to invade the imaged volume? While we cannot make definitive statements about events outside of the field of view, numerical considerations make this latter scenario unlikely. Within the imaged volume, 13 weeks after PCA treatment, there are an average of 123.6 ± 14.2 new axons, but only 15.4 ± 2.7 sprouted axons and of those sprouted axons, only 4.4 ± 0.9 exit the imaged volume. Because some sprouted axons branch and both branches can exit the imaged volume, the average total number of sprouted axon exit events is slightly higher, 5.3 ± 1.2. Thus, for sprouted axons outside of the imaged volume to account for the new axons we see invading the imaged volume, the sprouting rate in adjacent regions would have to be consistently ~23-fold higher than in the imaged volume. While this is formally possible, we favor the more parsimonious explanation, consistent with the immunohistochemical images of the entire forebrain (Figures 1 and 2) that new axons originate from deeper structures and represent some form

of long-distance regrowth. What we can't determine definitively is whether these new axons ultimately originate from the neurons that sustain damage or from uninjured neurons.

The new axons that repopulate the field of view are not transient structures: Of the new axons present 6 weeks after PCA treatment, 100 % are still present at week 19. Thus, it appears that recovery of serotonin axons does not result from overgrowth followed by pruning, at least within our 29 week-long maximum monitoring period. This pattern is similar to the initial development of serotonin fiber innervation of the neocortex in late embryonic and early postnatal life which also lacks significant overgrowth and pruning (Lidov and Molliver, 1982).

Might the stress of PCA treatment cause Slc6a4-EGFP neurons to change their transmitter phenotype? To address this question we performed *in vivo* time-lapse imaging weekly following PCA treatment, sacrificed the mouse and processed the somatosensory cortex for immunohistochemistry with an antibody directed against the serotonin transporter. When the field of view from the *in vivo* imaging was recovered, it was revealed that surviving, sprouted and new axons were all serotonin-transporter immunopositive (Figure S6), arguing against a change in neurotransmitter phenotype.

Regrowing serotonin axons have normal morphology and distribution

Examination of exemplar images indicates that the new axons repopulating the field of view following PCA treatment do not grow along surviving axons nor are they guided by blood vessels (Figure 3 and Figure 4). The former conclusion is supported by an analysis of axon neighbor relations (Figures 5A and 5B). When the distance to the nearest axon is calculated for every point along every axon in the field of view, we found that PCA treatment increases the mean distance to the nearest neighbor by a factor of 2.39 ± 0.18 at week 1 (compared to the pre-treatment time-point at −1 week) and this distance decreases gradually as the field of view is repopulated with new axons (a factor of 1.36 ± 0.07 at week 19). Importantly, a histogram showing the distribution of nearest neighbor distances fails to show a peak at distances < 1 μm at any time point, indicating that serotonin axons rarely contact each other as would be expected if the surviving axons served as a scaffold for new axons. In fact, the changes in the nearest neighbor histogram after PCA treatment are most consistent with a model in which new axons actively avoid contact with surviving axons, sprouting axons or each other.

When new axons enter the field of view after PCA treatment they generally recapitulate the morphology of both surviving axons and control saline-treated axons. Figure 5C shows that the tortuosity of new axons is similar to that of these other populations (tortuosity ratio of new axons at week 19 is 1.18 ± 0.02 compared with 1.16 ± 0.04 for surviving PCA-treated axons at week 19 and 1.12 ± 0.01 for surviving saline-treated axons at week 19). Likewise, the density of axonal varicosities in new axons is similar to surviving axons and saline-treated controls (week 19: survived: 0.43 ± 0.01 varicosities/μm; new: 0.42 ± 0.01; $p = 0.58$).

Regrowing serotonin axons do not extend along pathways previously established by degenerated fibers

When new axons enter the field of view, do they grow along pathways that had previously been established by degenerated fibers? Casual observation of the trajectories of new axons suggests that they do not (Figure 3A). To quantitate this impression, an overlap index was calculated in which each new traced axon at week 27 was separately scored for overlap in 3-D space with each traced degenerated axon present at week -1 in two different PCA-treated mice. We set a criterion that >80% of the points along a new axon must overlap those of a degenerated axon in order for the axon to be scored as overlapping. We further set the overlap scoring zone to have a radius of 4.5 μm around each point in the new axon to account for small changes in the geometry and orientation of the imaged volume over 29 weeks. This analysis showed that only 3% of the new axons overlapped with degenerated axon pathways. These parameters are valid because when they are applied to compare surviving axons at week 27 with the same axons at week −1, 96% of the surviving axons are scored as overlapping. Thus very few axons grow along pathways abandoned by degenerating axons. Indeed, it is possible that even the 4% positive score for new axons represents new axons are that are growing close to, but not precisely along the pathways of degenerated axons, since the limits of our imaging technique do not allow us to make this distinction. Importantly, these results further argue against a model in which intact serotonin axons are merely depleted of serotonin by PCA treatment (or depleted of EGFP in Slc6a4-EGFP mice) and then slowly refill as this mechanism would be expected to yield a high degree of overlap between new axons and “degenerated” axon pathways.

The location in 3-D space of axons was calculated as a distribution of probability densities in three dimensions for both PCA and saline treated mice (Figure S7). In saline-treated mice, these 3-D axon distributions were remarkably stable across time (from −1 to 21 weeks), consistent with stable exemplar images (Figure 3). In PCA-treated mice, these distributions were also remarkably similar, even though PCA produced a large reduction in axon density followed by a slow recovery. This consistency indicates that, even though the new axons do not grow in the exact same locations where degenerated axons previously ran, overall, the new axons that underlie recovery after PCA recapitulate the 3-D axon distribution density of the pre-lesion state.

Morphological or positional properties cannot be used to predict which axons will survive PCA treatment

Are there any morphological or positional criteria that can be used to predict which axons will survive PCA treatment? Axons at the week −1 pre-treatment time-point were divided into two groups- those that would later survive PCA treatment and those that would degenerate. When these groups were compared, neither tortuosity nor varicosity density differed between them (tortuosity of surviving axons was 1.15 ± 0.01 compared with 1.16 ± 0.0 for those which would later degenerate; varicosity density of surviving axons was 0.44 ± 0.02 varicosities/μm compared with 0.42 ± 0.01 for those which would later degenerate). In addition, the finding that 3-D axon distribution density was not affected by PCA treatment (compare week −1 and week 1; Figure S7) suggests that an axon’s position in 3-D space within our imaging volume was not a predictor of whether it would survive.

Regrowing serotonin axons are functional and might contribute to behavior

We have shown that the new axons that enter the field of view following PCA treatment are serotonin transporter-immunopositive (Figure S6), express a normal density of axonal varicosities and recapitulate the overall spatial distribution of pre-lesion axons (Figures 5 and S7). However, this does not prove that these axons have the capacity to release serotonin when action potentials invade. To address this question, a stimulating electrode was placed in the medial forebrain bundle of anesthetized serotonin-transporter-EGFP mice and a carbon fiber microelectrode for serotonin fast-scan cyclic voltammetry (FSCV) (Hashemi et al., 2012; Wood and Hashemi, 2013) was placed in layer 1 of the somatosensory cortex. Serotonin release was evoked by a train of pulses (120 pulses at 60 Hz and 350 μA) as shown in the color plot in Figure 6A. FSCV color plots represent a grouping of individual cyclic voltammograms, collected every 100 ms with current in false color. A cyclic voltammogram collected towards the end of the stimulation identifies serotonin via the discrete position of redox peaks (Figure 6A, inset). The current vs. time taken at the peak oxidation current is directly convertible to serotonin concentration vs. time. In saline treated mice, peak evoked serotonin release was measured at 1 week (9.4 ± 1.5 nM, n = 2), 3 months (26.0 ± 6.4 nM, n = 2) and 6 months (14.5± 8.3 nM, n = 2) after treatment. Serotonin levels and release-uptake profiles are within the characteristic range previously reported in mice (Wood and Hashemi, 2013). By contrast, no evoked serotonin release was detected 1 week or 3 months after PCA treatment (n = 6 and 4, respectively). However, 6 months after PCA treatment, a recovery of evoked serotonin release was evident (11.9 ± 2.9 nM, n = 4). By comparison, the total length of serotonin axons has recovered from its nadir of 25.5 ± 3.5% of baseline at week 1 to 53.8 ± 3.4% at 3 months and 68.0 ± 6.7% at 6 months. A likely reason for the lack of signal at 3 months is that evoked serotonin was below our limit of detection. Alternatively, new serotonin axons in the somatosensory cortex at 3 months after PCA are present but may require further maturation to release serotonin in response to electrical stimulation.

Prior work has shown that attenuation of the serotonin system can result in behavioral hyper-reactivity (Jacobs et al., 1975). We found that PCA treatment produced significant increases in the amplitude of acoustic startle responses in comparison to saline-treated controls, measured 1 week after treatment (saline: 85.3 ± 21.2 arbitrary startle force units in response to 120 db tone, n = 10; PCA 143 ± 33.3 units, n = 10; $p = 0.00478$; Figure 6B). However, 6 months after treatment, no difference between the saline and PCA-treated groups was found (saline: 70.3 ± 22.8, n = 9; PCA: 58.8 ± 8.4, n = 10; $p = 0.872$). Likewise, in a forced swim test, PCA treatment decreased the amount of time spent immobile in comparison to the saline group at 1 week after treatment (saline: 92 ± 6.8 sec, n = 10; PCA: 64.7 ± 9.1 sec; n = 10; $p < 0.05$, Figure 6B). Again, 6 months after treatment, no difference could be seen between these groups (saline: 65.7 ± 9.7 sec, n = 9; PCA: 62.4 ± 11.8 sec, n = 10; $p > 0.05$). The degeneration of serotonin–EGFP axons by PCA treatment was confirmed with immunohistochemistry for both voltammetry and behavioral experiments (not shown). Might these behavioral effects result from PCA damage to dopaminergic neurons? To determine whether PCA treatment also injured dopamine neurons, we performed immunohistochemistry using antibodies directed against tyrosine hydroxylase. No damage to dopamine neuron cell bodies in the ventral tegmental area or dopamine axons in the

dorsal striatum or somatosensory cortex was observed (Figure S8). Thus, 6 months after PCA treatment, when significant recovery of serotonin innervation has occurred (Figures 2 and 3) and this recovery was sufficient to restore evoked serotonin release as determined using voltammetry (Figure 6A), both of these behavioral measures normalized to control levels (Figure 6B). Of course, the recovery of serotonin release and the recovery of these behavioral measures 6 months after PCA lesion is a mere correlation at this point and there is no proof that they are causally related.

Serotonin axons regrow from severed ends following a neocortical stab injury

Is the extensive regrowth of serotonin axons seen following PCA lesion a general property of serotonin axons or some specific response to pharmacological injury that would not be seen with traumatic injury? To address this question, we employed a cortical stab protocol. Adult mice, which had received craniotomies overlying the right somatosensory cortex, were challenged by brief stereotaxic insertion to a depth of 2 mm of a miniature surgical blade, 1.2 mm wide. The blade was oriented with the width running in the coronal plane so that the resultant stab wound would transect most of the serotonin axons, which generally run in a rostrocaudal course in this region. Figure 7A shows an exemplar mouse in which in vivo 2-photon imaging of serotonin axons was performed immediately before and ~ 1 hour after the stab injury. This treatment was followed by implantation of a cranial window and regular weekly monitoring for 18 weeks. One hour after stab injury, 36 randomly-selected cut ends of axons were traced at the rift edge. By 1 week after injury, 25 of these cut ends displayed new axon growth, a value which increased to 29 and then 31 at 9 and 18 weeks, respectively. In addition, some of the regrown axons growing from the cut ends at the rift edge formed new branchpoints: there were 4, 20 and 27 new branchpoints at 1, 9, and 18 weeks after the stab lesion, respectively. When total axon length within the rift was measured for this mouse there was 20.6 mm before the stab lesion and 0 mm ~1 hour afterwards. One week after the stab there was 4.2 mm of axonal length present and this value increased to 11.2 and 16.3 mm at 9 and 18 weeks, respectively (Figure 7B). In the population of 6 mice, in which serotonin axons were completely ablated within the stab rift, there was some recovery evident even after 1 week (17.8 ± 5.5 % of baseline rift axon number) and substantial recovery after 18 weeks (81.0 ± 7.4%; Figure S9). Thus, the stab wound severs serotonin axons but the cut ends of the axons do not appear to persistently regress more than a few microns. This stands in notable contrast to PCA treatment in which the damaged axons regress beyond the field of view with in vivo imaging and likely regress all the way to the caudal medial forebrain bundle.

At 18 weeks after the lesion, 28/36 traced severed ends showed new growth (Figures S9C and S10). That growth ranged from 12 – 877 μm with a mean of 182 μm. Of the 28 severed ends of axons that showed new growth, 7 were able to traverse the stab rift completely and emerge on the other side. In 11/28 severed axons, the regrown portion of the axon exited the field of view so the values here represent only a lower bound of the distance. There are also new segments of serotonin axon within the rift that cannot be traced to cut ends within the imaging volume. These may derive from sprouting of neighboring uninjured axons or they may be growth from the ends of cut axons that are present just outside of the imaging volume.

To further test the hypothesis that serotonin axons regrow following neocortical stab injury, the same stab protocol was employed but was followed, at various durations by EGFP immunohistochemistry to reveal serotonin axons together with NeuN immunohistochemistry which labels neuronal nuclei. This technique relies upon between-animal comparisons, but has the advantage that it allows for visualization of all of the cortical layers. Sagittal sections were prepared from a region of somatosensory cortex centered upon the medio-lateral extent of the stab rift to avoid rift edge effects (Figure 8A). Sections from mice sacrificed 1 hour after the stab lesion reveal a broad rift, devoid of tissue, ~ 150 μm wide, extending from the brain surface, through all 6 cortical layers, to the underlying white matter. Within approximately 100 μm of the rift edge, on both sides, serotonin axons are mostly swollen and fragmented, while those further away appear morphologically normal.

When mice were sacrificed 1 week after the stab injury, the rift zone was still discernable as a region of diffuse NeuN immunoreactivity, but the tissue appears to have knit together to partially repair the rift. While there were 194 ± 9 axons in the rift volume in control mice (n=8) and this was, of course, reduced to zero in mice sacrificed 1 hour after the stab injury (n=4), progressive recovery was seen beginning at one week (25 ± 1 axons, n=9 mice) and continuing at three months (62 ± 4 axons, n=5) and six months (76 ± 3 axons, n=10; Figure 8B). An even greater degree of recovery was seen when using a measure that approximates total serotonin axon length within the rift (% area occupied by axons in the rift zone; Figure 8B). Growth of serotonin axons into the rift zone proceeded similarly in layer 1 which has very few neuronal cell bodies, and layer 5, which has many neuronal cell bodies.

A caveat should be sounded about the apparent cell-free rift in the tissue evident 1 hour after the stab lesion (Figure 8A). While similar rifts were observed in tissue sections from 4/4 mice, it is possible that these rifts are expanded by the mechanical stress of tissue slicing and processing. While it is likely that a cell-free zone is present at this point in vivo, its width may not be accurately measured in these fixed tissue sections.

Serotonin axons fail to regrow after discrete laser axotomy

Previous work has used a high-energy pulsed tuned infrared laser to sever individual GFP-labelled glutamatergic axons in the adult mouse neocortex (Canty et al., 2013). Ablation of either pyramidal cell or thalamo-cortical axons with a laser microlesion, produced a small degree of retraction of the proximal axon, followed by little or no regrowth from the severed end when monitored for up to an entire year. This failure to regrow was seen even though the microlesions did not create a persistent glial scar (Canty et al, 2013).

Here, we have applied this technique to serotonin axons running in layer 1 of the neocortex and have found nearly identical results: in 7/7 mice, laser lesions of a single axon produced retraction over a distance of ~10 – 30 μm followed by a complete failure to regrow from the severed end. Figure S11 shows and exemplar experiment in which a single serotonin-EGFP axon was ablated leaving neighboring serotonin-EGFP axons intact (although presumably some neighboring unlabeled axons and other neuronal and glial structures are damaged as well). The surviving portion of the presumably proximal axon was swollen 1 day after the lesion, but at 4 days after the lesion had returned to a superficially normal appearance with typical diameter and varicosity density. However, the severed end of this axon was then

entirely static, exhibiting no further elongation or retraction over a 16 week monitoring period. In sum, while profound serotonin axon regrowth was seen following PCA or neocortical stab lesions, ablation of a single serotonin-EGFP axon did not produce either regrowth from the severed end or sprouting of neighboring intact serotonin-EGFP axons. It is unclear why laser axotomized serotonin axons fail to regrow while stab-lesioned axons succeed. One possibility is that the process of laser axotomy locally disrupt the structure of the serotonin axon or the perhaps the extracellular matrix in a manner that persistently blocks regrowth. Another possibility is that serotonin axon regrowth requires a threshold level of damage to be evoked and the small laser lesions used herein are below this threshold.

Discussion

The present work shows that serotonin axons in the brain have the unusual property to undergo regrowth following damage produced by either a systemic amphetamine lesion or a local stab lesion. Following PCA lesion, the new axons largely recapitulate the morphology (varicosity density, tortuosity), neighbor relations and layer-specific distribution of pre-lesion axons. Like uninjured axons, they are serotonin-transporter immunopositive. However, unlike regrowing axons in the peripheral nervous system, they do not follow pathways in the tissue matrix that are left behind by previously degenerated axons.

New axons that emerge following PCA lesion do not demonstrate overgrowth or pruning. They persist for at least 6 months. Furthermore, at the 6 month post-lesion time-point, have the capacity to release serotonin in response to electrical stimulation. These findings are consistent with previous reports showing that axons of serotonin neurons in the caudal raphe complex are among the first to cross a grafted and chondroitinase-treated spinal cord lesion in mouse models and can contribute to restoration of locomotion (Kanno et al., 2014) bladder and diaphragm control (Alilain et al., 2011; Lee et al., 2013).

Surprisingly, sprouting of uninjured axons within the field of view does not substantially contribute to the recovery of serotonin axons density following PCA lesion. In fact, the rate and extent of local sprouting is the same in PCA-treated and control serotonin axons. The particular serotonin axons that survive PCA treatment cannot be predicted on the basis of their location, neighbor relations, tortuosity or varicosity density.

The regrowth of serotonin axons following a neocortical stab extends these findings in two important ways. First, it establishes that regrowth of damaged serotonin axons is not a unique feature of amphetamine lesions. Second, because the damaged axons almost entirely remain within the field of view for in vivo imaging, this allows us to assess the state of the severed ends of damaged axons. Here, the result is clear. A large fraction (>80 %) of the severed ends of serotonin axons display new growth and in many cases this regrowth is sufficient to completely cross the stab rift. Thus, the long-held view that axons in the brain fail to undergo regrowth following injury does not hold for serotonin neurons that innervate the neocortex.

The inflammatory response produced by amphetamine lesion is transient and, unlike concussive or penetrating brain injury, no glial scar is produced (Wilson and Molliver, 1994). Nonetheless, it appears that serotonin axons have the ability to penetrate glial scars in the brain (such as those produced following a thermal lesion; Hawthorne et al., 2011) and hence are likely to demonstrate regrowth and recovery of function following a broad array of brain injuries. Our own findings show that stab injury produces local astrocyte activation, as indexed by GFAP immunoreactivity, that persists for at least 10 weeks and that regrowing serotonin axons crossing the stab rift can run adjacent to these activated astrocytes (Figure S12). This finding is consistent with the previous observation in raphe spinal serotonergic axons that occasional regenerating axons can pass through GFAP-positive tissue bridges that form following complete spinal transection (Lee et al, 2010). One important implication of these findings is that the tissue matrix of the adult central nervous system, generally thought to be non-permissive for axonal growth (Chew et al., 2012; Tuszynski and Steward, 2012), fails to inhibit regrowth of serotonin axons.

Why are serotonin axons able to regrow in the adult brain when almost all other axons fail? One functional explanation is that, since serotonin axons in the brain mostly operate through slow, diffuse volume transmission rather than fast, localized synaptic transmission, constraints on the spatial fidelity of regrowth are relaxed: Unlike a glutamate-releasing axon which forms conventional synapses, a serotonin-releasing axon needs only to achieve reinnervation of its approximate former position in order to restore functional volume signaling.

One possible molecular explanation (of many) is that, unlike the growth cones of glutamate axons, serotonin axonal growth cones fail to receive the stop signals from the tissue matrix that inhibit other axonal types. Ultimately, single–cell expression profiling of pre-lesion and regrowing serotonin neurons in the raphe complex will be useful to address this question as will inducible deletion in the adult brain of candidate axon growth promoting genes within serotonin neurons. Perhaps, uncovering the unique molecular properties of regrowth-competent serotonin axons and the discovery of genetic and pharmacological manipulations that enhance or suppress long-distance serotonin axon regrowth will allow for the development of therapies to promote axon regrowth in a wide variety of cell types.

Experimental Procedures

Transgenic mice

Slc6a4-EGFP BAC transgenic mice were made by Charles Gerfen (NIH) as part of the GENSAT consortium (line RP23-39F11, BAC BX86, RRID: MMRRC_030692-UCD). Slc6a4-EGFP BAC-Cre mice created by the GENSAT consortium and purchased from the Mutant Mouse Regional Resource Center at U.C. Davis (stock #031028-UCD and #017260-UCD, RRID: MMRRC_031028-UCD and MMRRC_017260-UCD). All experiments were approved by the Animal Care and Use Committees of The Johns Hopkins University, or for the voltammetry studies, Wayne State University.

Surgical procedure for *in vivo* imaging

A craniotomy was made overlying the right somatosensory cortex in adult Slc6a4-EGFP mice and serotonin axons in layer 1 were imaged with a two-photon microscope using 920 nm laser illumination. Mice, aged 4 to 5 months, were anesthetized with 1–2% isoflurane and placed in a stereotaxic device (Stoelting). A small dose of dexamethasone (0.04 ml at 2 mg/ml) was administered by subcutaneous injection prior to surgery to minimize potential swelling at the surgical site and a subcutaneous injection of buprenorphine (0.3 mg/ml) was also given before surgery to alleviate pain. The skull was exposed with a midline scalp incision and a region (2 × 2 mm) over somatosensory cortex based on stereotaxic coordinates was carefully removed using a #11 surgical blade (the medial, anterior corner of the craniotomy was located 0.5 mm posterior and 1.0 mm lateral to bregma). During cutting of the craniotomy, the skull was bathed in saline to minimize damage to underlying structures. Surgifoam (Johnson & Johnson) soaked in ACSF was used to stop bleeding from the surrounding tissue. A square fragment of cover slip glass was placed inside the walls of the craniotomy and Metabond cement (Parkell, Edgewood, NY) was applied at the edges to form a cranial window and to fasten a laterally-protruding stainless steel plate. Following surgery, Baytril (2.5 mg/kg, delivered by subcutaneous injection) was given as antibacterial prophylaxis.

In vivo imaging of serotonin axons

For *in vivo* imaging, mice were anesthetized with 1–2% isoflurane and placed on a feedback-controlled warming pad. The stereotaxic microscope stage was equipped with lateral bars which fastened to the mouse's headplate for stabilization. The stage was fixed on an x–y translator under a laser-scanning confocal microscope (Zeiss LSM 510 NLO) equipped with a 40X W Plan-Apochromat VIS-IR water immersion objective (Zeiss, 1.0 NA) and a non-descanned photomultiplier tube attached to the epifluorescence port. Two-photon excitation (920 nm) was provided by a Chameleon vision II mode-locked Ti-Sapphire laser (Coherent). Z-stacks were acquired starting at the cortical surface and continuing to a depth of ~100 – 200 μm with a step size of 1 μm. Each stack was imaged with a resolution of 1024 × 1024 pixels (0.31 μm/pixel; pixel dwell time = 3.2 μsec).

PCA and saline injection protocols

Male and female mice, aged 4 to 5 months, were given *para*-chloro-amphetamine (PCA, Sigma-Aldrich; 20 mg/kg) or saline intraperitoneally in single-housed standard cages maintained at an ambient temperature 25 to 26 °C with continuous airflow. Injections were performed two times per day for four days. On a single day the injections were given 6 hours apart and the interval between the second injection on one day and the first injection on the next day was 16 hours.

Virus injection

Serotonin axons were labeled by dorsal raphe injection of AAV5-EF1a-DIO-hChR2(H134R)-EYFP-WPRE-pA. Adult serotonin transporter cre mice (4–5 months old) were anesthetized with 1–2% isoflurane and placed in a stereotaxic device (Stoelting). A glass pipette with 40 μm tip diameter was filled with mineral oil and connected to Nanoject

II (Drummond Scientific Company, Broomall, PA). The tip of the glass pipette was then front-filled with ~1 μl of AAV5-EF1a-DIO-hChR2(H134R)-EYFP-WPRE-pA. Injections were made 4.7 mm posterior from bregma, at a depth of 2.8–3.2 mm. A dye volume of 0.1–0.2 μl was delivered with a Nanoject II over a 10 min period. The pipettes were left for 15 min before they were withdrawn. The virus was developed in Karl Deisseroth's lab (http://www.med.unc.edu/genetherapy/vectorcore/research-grade/in-stock-aav-vectors/deisseroth) and purchased from UNC Vector Core.

Stab injury

A craniotomy was made overlying the right somatosensory cortex in adult Slc6a4-EGFP mice as described. A miniature blade (Surgistar, USM 6700) was placed on the dura of the somatosensory cortex with a stereotaxic device in a location that was roughly centered in the window but chosen to avoid major surface blood vessels. The blade was then was slowly advanced into the brain to the depth of 2 mm. Surgifoam (Johnson & Johnson) soaked in ACSF was used to stop bleeding from the surrounding tissue. A square fragment of cover slip glass was placed inside and sealed with Metabond dental cement (Parkell).

Laser axotomy

Laser-induced axon ablation was achieved by focusing a parked pulsed two-photon laser beam on a spot at a depth of 50 – 100 μm beneath of pial surface of the somatosensory cortex and illuminating for for 1 second. The wavelength used for laser axotomy was 850 nm and the power at the back aperture of the objective was ~100 mW. Lesions locations were chosen to avoid blood vessels and a single lesion was made per mouse.

Immunohistochemistry

The mice were anesthetized with ketamine (100 mg/kg) and xylazine (10 mg/kg) and perfused intracardially with phosphate-buffered saline (PBS) followed by 4% paraformaldehyde in PBS at 4 °C. The entire brain was removed and fixed in 4% paraformaldehyde for 3 hours at room temperature and then cryoprotected in 15% sucrose in PBS overnight at 4 °C, followed by a switch to 30% sucrose on the next day and continuing overnight. Sections of the mouse brain (40 μm thick) were prepared using a microtome and were washed with PBS and then blocked with 5% normal goat serum (Jackson ImmmunoResearch Laboratories #005-000-001, RRID: AB_2336983) and 0.3 % Triton X-100 in PBS for 2 hours at room temperature. The sections were incubated in primary antibody diluted in blocking buffer, overnight at 4 °C. The primary antibodies used were rabbit anti-5HT (1:20,000, ImmunoStar #20080, RRID: AB_572263), guinea pig anti-SERT (1:1,000, Frontier Institute #HTT-GP-Af1400, RRID: AB_2571777), rabbit anti-TPH2 (1:800, Millipore #ABN60, RRID: AB_11212793), rabbit anti-TH (1:1,000, Millipore #AB152, RRID: AB_390204), mouse anti-NeuN (1:500, Millipore #MAB377, RRID: AB_2298767), mouse anti-GFP (1:5000, Life Technologies #A11120, RRID: AB_221568), chicken anti-GFP (1:5000, Aves Labs #GFP-1010, RRID: AB_2307313), and rabbit anti-Glial Fibrillary Acidic Protein (1:1,000, Millipore #AB5804, RRID: AB_10062746). The sections were then washed with PBS and incubated in the secondary antibody in blocking buffer for 2 hours at room temperature. The secondary antibodies used were Cy3-labeled goat anti-rabbit (1:800, Jackson ImmunoResearch Laboratories #111-165-003, RRID:

AB_2338000), Cy3-labeled goat anti-guinea pig (1:800, Jackson ImmunoResearch Laboratories #106-165-003, RRID: AB_2337423), Cy3-labeled goat anti-mouse (1:800, Jackson ImmunoResearch Laboratories #115-165-062, RRID: AB_2338685), Cy5-labeled goat anti-mouse (1:200, Jackson ImmunoResearch Laboratories #115-175-146, RRID: AB_2338713), FITC-labeled goat anti-mouse (1:800, Jackson ImmunoResearch Laboratories #115-095-003, RRID: AB_2338589) and Alexa Fluor 488-labeled goat anti-mouse (1:1000, Life Technologies #A11039, RRID: AB_142924). Then, we mounted the sections on slides, and images were acquired using a single-photon confocal microscope (Zeiss).

Fast-scan Cyclic Voltammetry

Mice were terminally anesthetized with urethane (25% dissolved in 0.9% sodium chloride). Mouse body temperature (37° C) was maintained by placing a heating pad (Braintree Scientific) under the mouse throughout the duration of the experiment. A bipolar stimulating electrode (Plastics One, VA) was implanted into the MFB (AP: −1.58, ML: 1.10, DV: −4.8 – 5.0) and a Nafion-coated carbon fiber microelectrode was lowered into the somatosensory cortex (AP: −1.0, ML: +2.0, DV: −0.2 – 0.5). A Ag/Ag Cl reference electrode was placed into the contralateral hemisphere. The carbon fiber microelectrode was prepared thus: a single carbon fiber (T- 650; diameter: 7μm; Goodfellow, PA) was aspirated into a glass capillary (external diameter: 0.6 mm, internal diameter: 0.4 mm; A-M Systems) which was then pulled apart under heat and gravity. The protruding portion of the carbon fiber was cut under an optical microscope to a length of 50 – 100 μm. An electrical connection was forged with conductive epoxy and Nafion electroplating was applied. A PCIe-6341 DAC/ADC card (National Instruments, TX) generated an electrochemical waveform (1000 V s^{-1} at 10 Hz from −0.1 V to 1.0 V, resting at 0. 2 V). 120 biphasic electrical pulses were delivered to the stimulating electrode through a linear constant current stimulus isolator (NL800A Neurolog, Digitimer Ltd, AL) at 60 Hz, 350 μA and 2 milliseconds per phase. A CHEM-CLAMP potentiostat (Dagan Corporation, MN) measured output current. Data were collected and analyzed using WCCV 3.0 (Knowmad Technologies LLC, Tucson, AZ). Data were background subtracted to remove a large capacitative current and then filtered at zero-phase using a fourth order Butterworth with a low pass of 5 kHz. A standard calibration factor for the serotonin waveform was utilized to convert current to serotonin concentration.

Acoustic startle response

Two identical startle chambers (San Diego Instruments Inc., San Diego, CA, USA) were used for measuring startle reactivity and plasticity. Each mouse was placed in a Plexiglas cylinder (2 cm in diameter) within each chamber. A loudspeaker mounted 24 cm above the cylinder provided broadband background noise and acoustic stimuli. Presentations of the acoustic stimuli were controlled by the SR-LAB software and interface system (SR-LAB 94.1.7.48), which also rectified, digitized and recorded responses from the accelerometer. The maximum voltages within 40-ms reading windows, starting at stimulus onset, were used as the measures of startle amplitudes. Sound levels were measured inside the startle cabinets using a digital sound level meter (Realistic, Tandy, Fort Worth, TX, USA). The accelerometer sensitivities within each startle chamber were calibrated regularly and were found to remain constant over the test period. Each acoustic startle experiment consisted of

several sessions. The startle responsiveness session was used to evaluate the effects of treatment on startle responsiveness and included a 5-min acclimatization period to a 70-dB background noise (continuous throughout the session), followed by the presentation of five 40-ms-long 100-, 110- or 120-dB white noise stimuli presented in a randomized manner with randomized intervals ranging from 5 – 25 sec. The data of the startle responsiveness session were analyzed using two-way repeated measures ANOVA with treatment and amplitude of tone as independent variables; and the amplitude of the startle as the dependent variable.

Forced swim test

Mice were placed into glass cylinders, 15×30 cm, filled with room temperature water to a level of 20 cm. Mouse behaviors were video recorded for 6 min. The records were analyzed by a blind observer for the duration of immobility defined as the absence of movements or the paddling with one hind leg to keep balance on the surface. The time of immobility was assessed for the last 4 min of the test using StopWatch+ software (CBN, Emory University, Atlanta, GA, USA).

Image analysis

In vivo images were deconvolved using AutoQuantX3 (Media Cybernetics, Rockville, MD) to reduce the shot noise in each optical plane. We performed axon tracing in three-dimensional image stacks using Imaris (Bitplane, South Windsor, CT), and their length and branch points were measured. 3-D Imaris tracings were then exported to Matlab (Mathworks) as a set of 3D points representing the axons. The distance between each point along an axon was 0.33 microns.

To compute the dimensional density distribution analysis, each plane (x/y/z) was cut into slices, 3 microns thick. The number of axonal points in each slice was counted and divided by the total number of points in the volume. For across-animal comparisons, each dimension (x/y/z) was trimmed to match that of the mouse with the smallest distance in each sample group. Each dimension was calculated separately.

For nearest neighbor analysis, the distance to the nearest point located on another axon was calculated. The nearest distance histogram shows the distribution of nearest distance values, normalized by the total number of points, with a bin size of 1. The normalized distance to nearest neighbor is the mean nearest distance of all points in the tracing, normalized by the mean nearest distance calculated for week −1.

The tortuosity index was defined the length of the axon divided by the Euclidean distance between the ends or branch points.

To calculate the axon overlap index, week −1 and week 27 images first had to be aligned in 3 dimensions. This was performed by picking 10 – 15 fiduciary points (such as distinct axonal branch points) and performing reiterated 3-D translation and rotation (with no warping) to minimize the least squared error for the offsets between the fiduciary points. Then, each new axon at week 27 was compared one-by-one with each axon that would later degenerate in the week −1 image. This was done by sequential analysis of points on the new

axon and determining if a degenerated axon fell within a sphere of radius 4.5 μm. If >80% of the points in a new axon overlapped with any one degenerated axon, then it was scored as positive in the overlap index. Axons with a 3-D length of <15 μm were excluded from the analysis.

Varicosity analysis was performed using custom written programs in Igor Pro (Wavemetrics, Lake Oswego, OR). Only axons longer than 15 μm were scored for varicosities. This criterion was used to remove axons that skirted the edges of the imaged volume. Due to the large number of 'will degenerate' axons in PCA treated animals, a random subset of these axons were scored for varicosity density (equal to the number of 'surviving' axons within each animal). Otherwise, all axons in PCA treated animals (both 'will degenerate' and 'new') were scored for varicosity density. Likewise, due to the large number of 'surviving' axons in Saline treated animals, a random subset (n = 20) of these axons were scored for varicosity density. Varicosities were automatically detected as intensity peaks along the backbone tracing of each axon. For each point in the tracing, a line (1.5 – 2.0 μm) was drawn perpendicular to the tangent and the maximum intensity along this line was extracted. Together, these maxima (one per point in the tracing) form a peak intensity ridge along the axon. Individual points in the tracing were excluded if the intensity profile in the tails of the perpendicular line did not enter the average background intensity for the stack, this usually occurred when other axons were in close proximity. Varicosities where then detected as peaks of intensity along this axonal intensity ridge. Varicosity peak detection along this axonal intensity ridge was done using a threshold corresponding to ~80% of the peak intensity in the stack and a refractory distance where once a varicosity was detected, no other varicosities were allowed for 5 pixels (~0.95 μm). All automatically detected varicosities were manually verified in the raw 3D image volume by scorers blind to the experimental condition. Each automatically detected varicosity was either accepted or rejected. Rejected varicosities were not included in further analysis. As each axon was interrogated for the validity of its automatically detected varicosities, missing varicosities were manually added. Missing varicosities normally occurred for points in the original tracing where the automatic varicosity detection had failed due to other axons in close proximity.

Fixed tissue images were analyzed using NIH Image J (http://rsb.info.nih.gov/ij/) and average pixel intensity and area occupied by EGFP signal were measured. All data are presented as mean ± s.e.m. Unless otherwise noted, *P* values were calculated using the t-test for independent samples.

Supplementary Material

Refer to Web version on PubMed Central for supplementary material.

Acknowledgments

These experiments were inspired by the longstanding investigations of our collaborator and dear colleague Mark Molliver, who died in 2012. We thank Charles Gerfen (NIH) and the GENSAT team for providing the Slc6a4-EGFP BAC transgenic mouse. Jeremiah Cohen's lab provided us with the virus AAV5-EF1a-DIO-hChR2(H134R)-EYFP-WPRE-pA and helped with injection techniques. Michele Pucak, Marija Vasiljevic, Elliot Stryker, Yaretson Carmenate, Isaac Bernstein and Jillian Lane helped with image analysis. Thanks to Joshua Crawford for guidance

with the behavioral experiments. Funding was from the Johns Hopkins University Brain Science Institute and NIH NS81467 (DJL), Wayne State University startup funds and NIH R01MH106563 (PH), NIH MH083728 and MH094268, NARSAD, Stanley Medical Research Institute (MP) and NIH F32 NS090822 (SED). The Johns Hopkins Imaging Core Facility, which aided this effort, is supported by NIH NS050274.

References

Adori C, Low P, Andó RD, Gutknecht L, Rap D, Takács J, Kovács GG, Lesch KP, Bagdy G. Ultrastructural characterization of tryptophan hydroxylase 2-specific cortical serotonergic fibers and dorsal raphe neuronal cell bodies after MDMA treatment in rat. Psychopharmacology (Berl). 1980; 213:377–391. [PubMed: 21052985]

Alilain WJ, Horn KP, Hu H, Dick TE, Silver J. Functional regeneration of respiratory pathways after spinal cord injury. Nature. 2011; 475:196–201. [PubMed: 21753849]

Azmitia E, Gannon P. The ultrastructural localization of serotonin immunoreactivity in myelinated and unmyelinated axons within the medial forebrain bundle of rat and monkey. J Neurosci. 1983; 3:2083–2090. [PubMed: 6604793]

Beaudet A, Descarries L. The monoamine innervation of rat cerebral cortex: synaptic and nonsynaptic axon terminals. Neuroscience. 1978; 3:851–860. [PubMed: 215936]

Canty AJ, Huang L, Jackson JS, Little GE, Knott G, Maco B, De Paola V. In-vivo single neuron axotomy triggers axon regeneration to restore synaptic density in specific cortical circuits. Nat Commun. 2013; 4:2038. [PubMed: 23799397]

Chew DJ, Fawcett JW, Andrews MR. The challenges of long-distance axon regeneration in the injured CNS. Prog Brain Res. 2012; 201:253–294. [PubMed: 23186719]

DeFelipe J, Jones EG. A light and electron microscopic study of serotonin- immunoreactive fibers and terminals in the monkey sensory-motor cortex. Exp Brain Res. 1988; 71:171–182. [PubMed: 3416948]

Fuller RW. Effects of *p*-chloroamphetamine on brain serotonin neurons. Neurochem Res. 1992; 17:449–456. [PubMed: 1528354]

Gong S, Zheng C, Doughty ML, Losos K, Didkovsky N, Schambra UB, Nowak NJ, Joyner A, Leblanc G, Hatten ME, Heintz N. A gene expression atlas of the central nervous system based on bacterial artificial chromosomes. Nature. 2003; 425:917–925. [PubMed: 14586460]

Hashemi P, Dankoski EC, Lama R, Wood KM, Takmakov P, Wightman RM. Brain dopamine and serotonin differ in regulation and its consequences. Proc Natl Acad Sci USA. 2012; 109:11510–11515. [PubMed: 22778401]

Hawthorne AL, Hu H, Kundu B, Steinmetz MP, Wylie CJ, Deneris ES, Silver J. The unusual response of serotonergic neurons after CNS injury: lack of axonal dieback and enhanced sprouting within the inhibitory environment of the glial scar. J Neurosci. 2011; 31:5605–5616. [PubMed: 21490201]

Hornung JP. The human raphe nuclei and the serotonergic system. J Chem Neuroanat. 2003; 26:331–343. [PubMed: 14729135]

Jacobs BL, Trimbach C, Eubanks EE, Trulson M. Hippocampal mediation of raphe lesion- and PCPA-induced hyperactivity in the rat. Brain Res. 1975; 94:253–261. [PubMed: 125140]

Kanno H, Pressman Y, Moody A, Berg R, Muir EM, Rogers JH, Ozawa H, Itoi E, Pearse DD, Bunge MB. Combination of engineered schwann cell grafts to secrete neurotrophin and chondroitinase promotes axonal regeneration and locomotion after spinal cord injury. J Neurosci. 2014; 34:1838–1855. [PubMed: 24478364]

Lee JK, Chow R, Xie F, Chow SY, Tolentino KE, Zheng B. Combined genetic attenuation of myelin and semaphorin-mediated growth inhibition is insufficient to promote serotonin axon regeneration. J Neurosci. 2010; 30:10899–10904. [PubMed: 20702718]

Lee YS, Lin CY, Jiang HH, Depaul M, Lin VW, Silver J. Nerve regeneration restores supraspinal control of bladder function after complete spinal cord injury. J Neurosci. 2013; 33:10591–10606. [PubMed: 23804083]

Lidov HG, Molliver ME. An immunohistochemical study of serotonin neuron development in the rat: ascending pathways and terminal fields. Brain Res Bull. 1982; 8:389–430. [PubMed: 6178481]

Mamounas LA, Altar CA, Blue ME, Kaplan DR, Tessarollo L, Lysons WE. BDNF promotes the regenerative sprouting, but not survival, of injured serotonergic axons in the adult rat brain. J Neurosci. 2000; 20:771–782. [PubMed: 10632606]

Marcusson JO, Ross SB. Binding of some antidepressants to the hydroxytrptamine transporter in brain and platelets. Psychopharmacology. 1980; 102:145–155. [PubMed: 2274599]

Molliver ME, Berger UV, Mamounas LA, Molliver DC, O'Hearn E, Wilson MA. Neurotoxicity of MDMA and related compounds: anatomic studies. Ann NY Acad Sci. 1990; 600:640–664.

Muller, CP.; Jacobs, B. Handbook of the Behavioral Neurobiology of Serotonin. New York: Academic Press; 2010.

O'Hearn E, Battaglia G, Souza EB, Kuhar MJ, Molliver ME. Methylenedioxyamphetamine (MDA) and methylenedioxymethamphetamine (MDMA) cause selective ablation of serotonergic axon terminals in forebrain: immunocytochemical evidence for neurotoxicity. J Neurosci. 1988; 8:2788–2803. [PubMed: 2457659]

Tsai HC, Zhang F, Adamantidis A, Stuber GD, Bonci A, de Lecca L, Deisseroth K. Phasic firing in dopaminergic neurons is sufficient for behavioral conditioning. Science. 2009; 324:1080–1084. [PubMed: 19389999]

Tuszynski MH, Steward O. Concepts and methods for the study of axonal regeneration in the CNS. Neuron. 2012; 74:777–791. [PubMed: 22681683]

Wilson MA, Molliver ME. Microglial response to degeneration of serotonergic axon terminals. Glia. 1994; 11:18–34. [PubMed: 8070892]

Wood KM, Hashemi P. Fast-scan cyclic volammetry analysis of dynamic serotonin responses to acute escitalopram. ACS Chem Neurosci. 2013; 4:715–720. [PubMed: 23597074]

Yoo M, Khaled M, Gibbs KM, Kim J, Kowalewski B, Dierks T, Schachner M. Arylsulfatase B improves locomotor function after mouse spinal cord injury. PLoS One. 2013; 8:e57415. [PubMed: 23520469]

Highlights

- We measured serotonin axons in vivo using 2-photon microscopy with brain injury.
- Amphetamine injury produced large retrograde degeneration followed by slow regrowth.
- Stab injury severed axons, which regrew from their cut ends across the stab rift.
- Regrowing axons did not use pathways left by degenerated axons to guide regrowth.

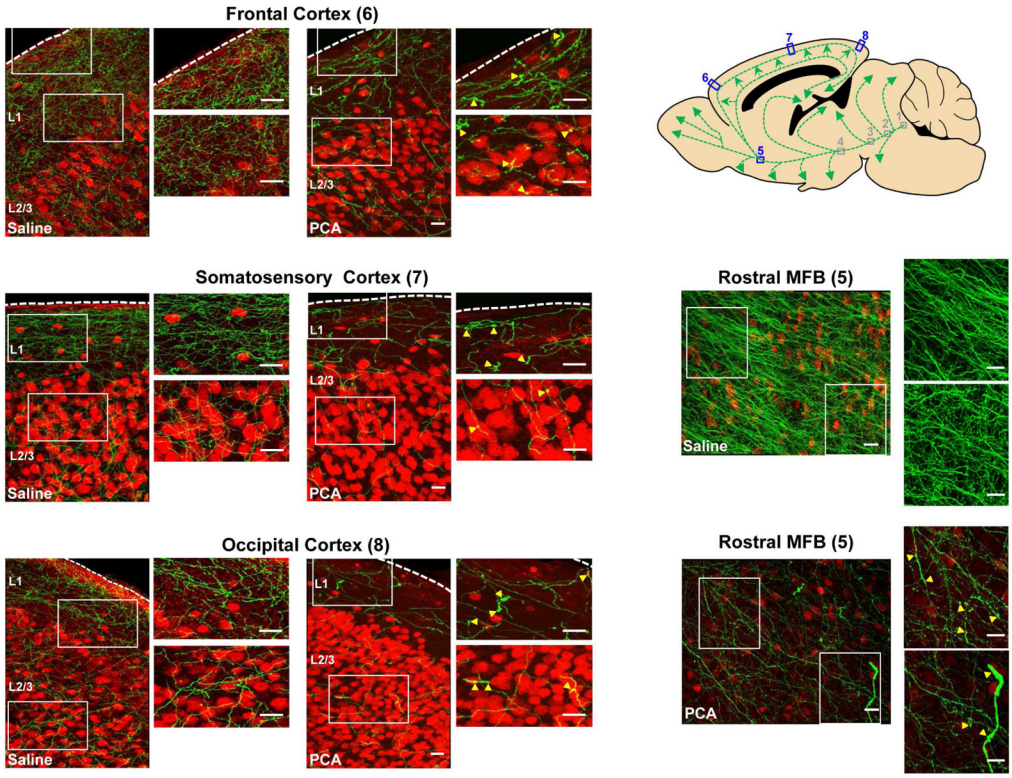

Figure 1. One day after PCA treatment, immunohistochemistry reveals swollen and fragmented serotonin axons in neocortical regions and the rostral MFB

Double-label immunohistochemistry was performed on sagittal sections of serotonin transporter-EGFP mice. These sections were also stained for NeuN (to mark a subset of neuronal nuclei, red). Yellow arrowheads indicate swollen axons. Scale bars = 20 μm.

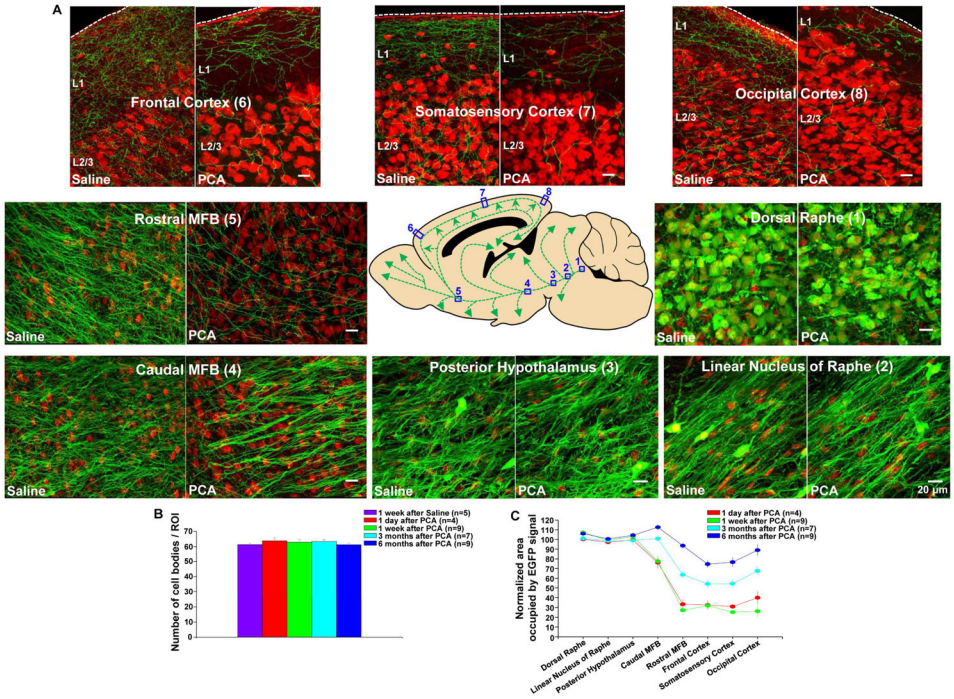

Figure 2. PCA treatment evokes retrograde degeneration of serotonin axons in the adult mouse brain as shown by immunohistochemistry

(**A**) In serotonin-transporter-EGFP mice, the serotonin axons were labeled with an antibody directed against GFP (green), and a subset of neurons were labeled with the nuclear marker NeuN (red) to provide landmarks. The central panel shows a schematic representation of the serotonin neurons of the dorsal raphe and their C-shaped projection to the neocortex in the sagittal plane. Each location along the pathway shows images taken 1 week after PCA or saline treatment. In PCA-treated mice, serotonin axons were lost in the most distal part of the projection including the occipital (8), somatosensory (7) and frontal (6) cortex as well as the rostral median forebrain bundle (MFB, 5). Serotonin cell bodies in dorsal raphe (1), axons in linear nucleus of raphe (2), and posterior hypothalamus (3) were unaffected.

(**B**) Serotonin cell body density in the dorsal raphe was not affected by PCA treatment in either short or long term measurements. Please note that the indicated times are after the end of the 4 day-long PCA treatment. Population data are presented as mean +/− standard error of the mean in this an all subsequent figures.

(**C**) Quantification of the normalized area occupied by the serotonin-EGFP signal at various time points after PCA and saline treatment shows partial recovery in the previously-depleted regions.

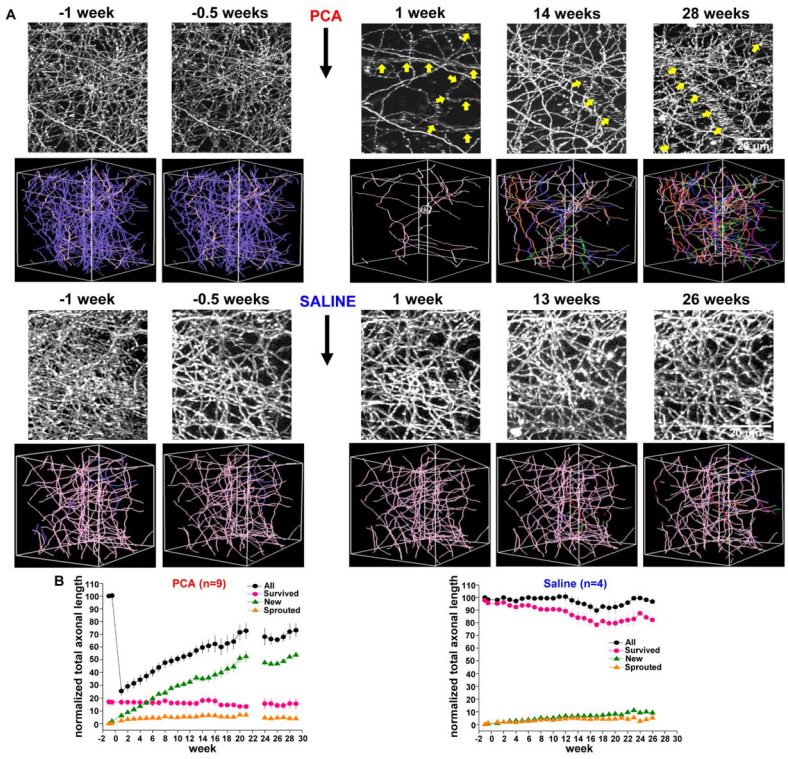

Figure 3. Long-term *in vivo* imaging reveals serotonin axon regrowth in the adult mouse brain

(**A**) Exemplar maximal z-projection (top) and 3D axonal tracing images (bottom) after PCA treatment show massive degeneration of serotonin axons and subsequent slow recovery over 29 weeks. Purple and pink color axons in 3D images indicate degenerated and survived axons, respectively. Each of the many other colors codes for the week of first appearance of a new axon entering the field of view (for example, new axonal segments appearing in week 6 are orange and those appearing in week 11 are red). Serotonin axons were highly stable in response to saline treatment. The tubular structures composed of many horizontally-elongated puncta in the z-stack images are blood vessels filled with serotonin-transporter-positive platelets (Marcusson and Ross, 1980). These blood vessels are indicated with yellow arrows.

(**B**) Population data for the measure of normalized total axonal length after PCA (n = 9) and saline (n = 4) treatment revealed that the recovery following PCA treatment is dominated by new axons.

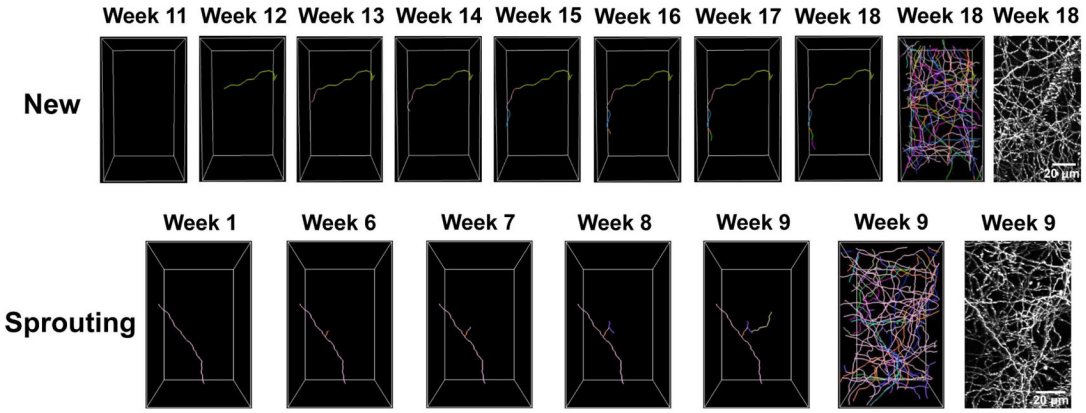

Figure 4. New and sprouting axons can be seen to gradually extend within the field of view

The top panels show an exemplar new axon. The new green axon appeared at week 12, and it continued extending through week 18. The bottom panel shows an exemplar sprouting axon. The pink axon in week 1 has survived PCA treatment. The sprout that extends from this surviving axons axon is first seen in week 6, and it gradually extends through week 9. For both the new and sprouting exemplars, the rightmost panels show a tracing of all axons and the maximal z-projection to provide context.

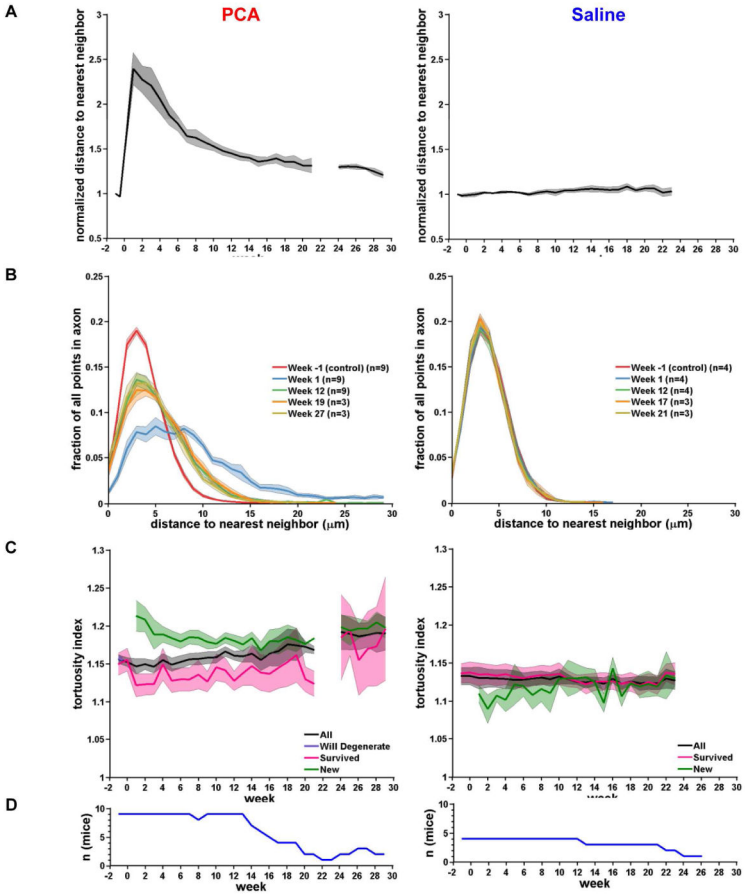

Figure 5. Following PCA lesion, new axons gradually achieve similar neighbor relations as compared to saline-treated control axons

(**A**) Average distance to nearest neighbor for all points in the axonal tracing, normalized to the average distance to nearest neighbor for week −1. In PCA treated mice (left panel), the distance to nearest neighbor approaches control levels as axons regrow. In saline treated mice (right panel), the distance to nearest neighbor remains stable. The shaded area represents the SE.

(**B**) Histograms of the distance to nearest neighbor for selected weeks. At week 1, the lower axonal density is reflected by an increase in each axons distance to its nearest neighbor. By week 27, as axons regrow, the distance to nearest neighbor is similar to control (week −1).

(**C**) Average tortuosity index (length of axon/Euclidean distance) contrasting all axons versus ‘will degenerate’, ‘survived’ and ‘new’. Note that ‘will degenerate’ is a single point at week −1 in PCA.

(**D**) Number of mice per week (n) for data plotted in panels A–C.

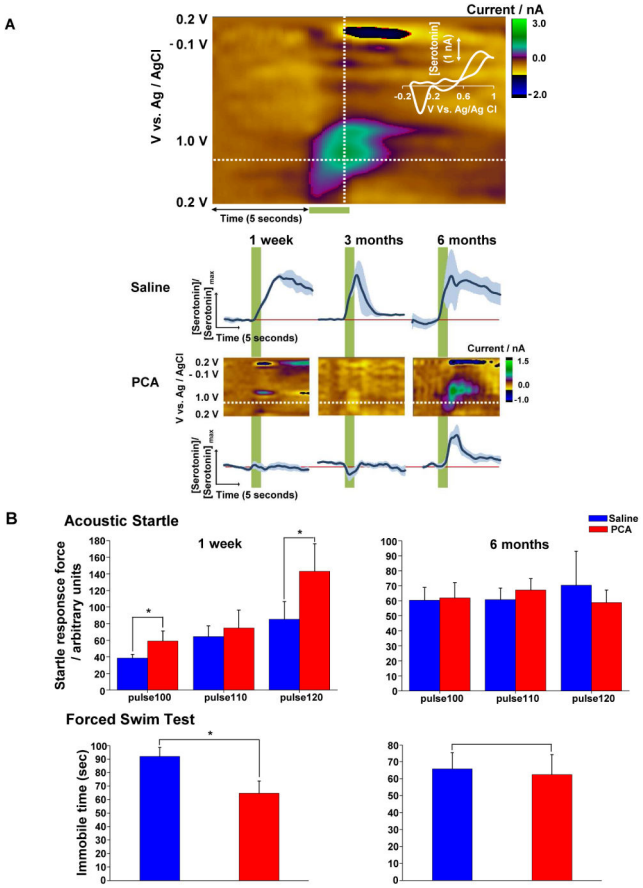

Figure 6. The slow recovery of neocortical serotonin innervation after PCA treatment is associated with the recovery of evoked serotonin release and behavioral changes

(**A**) Representative color plot from saline treated mouse (3 month) showing stimulation-evoked (120 pulses at 60 Hz) serotonin in the somatosensory cortex. Potential is on the abscissa, time on the ordinate and current is in false color. Stimulation of the MFB is indicated by the green bar under the color plot. Inset – a single cyclic voltammogram taken from the position of the vertical dashed line displaying characteristic serotonin redox peaks. Averaged, normalized $[serotonin]_{evoked}$ vs. time traces are shown in the bottom panels. These are derived from the positions denoted by the horizontal dashed lines in the color plots shown in the middle panels. Stimulation is indicated by the green vertical bar. (**B**) Acoustic startle and forced swim test indicate hyper-reactivity 1 week after PCA treatment when compared with the saline-treated group (n=10 for each group). At the 6-month time point, there was no significant difference between the saline (n=9) and PCA (n=10) groups for either test. *P < 0.05.

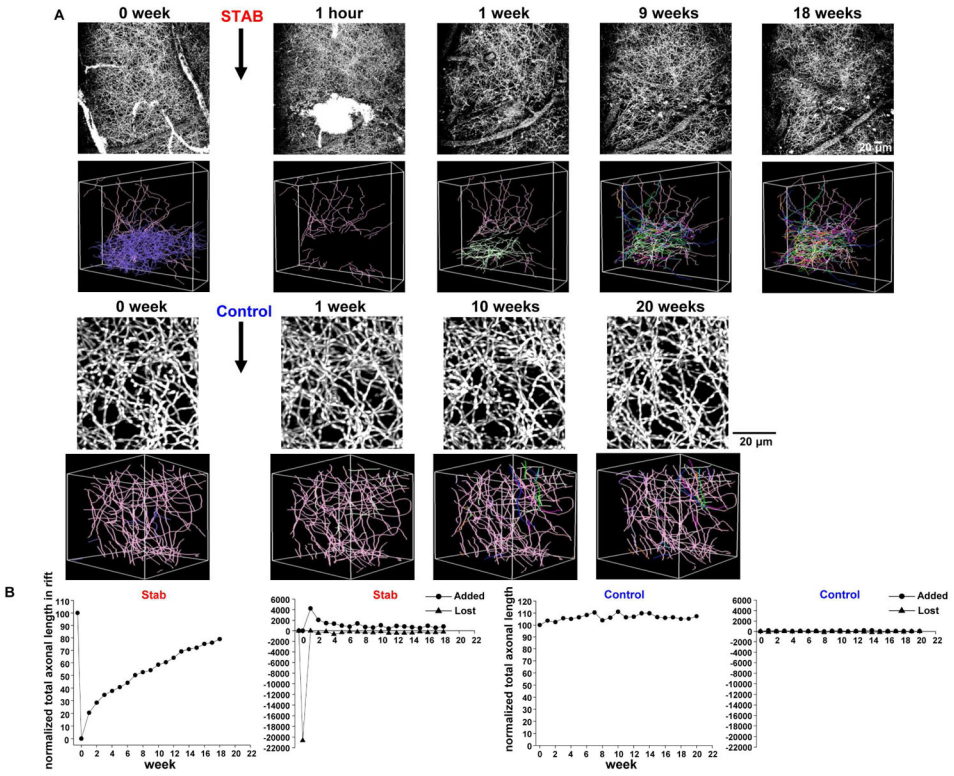

Figure 7. Long-term *in vivo* imaging reveals serotonin axon regrowth in the adult mouse brain after stab injury

(**A**) Exemplar maximal z-projection (top) and 3D axonal tracing images (bottom) after stab injury show significant degeneration of serotonin axons and subsequent recovery over 18 weeks. Purple and pink color axons in 3D images indicate degenerated and survived axons segments, respectively. Each of the many other colors codes for the week of first appearance of a new axon entering the field of view. Serotonin axons were highly stable in control mice. (**B**) Normalized total axonal lengths within the rift zone in the stab lesion (n=6) and control (n=4) groups are plotted. Total added and lost axonal length within the rift zone are also shown.

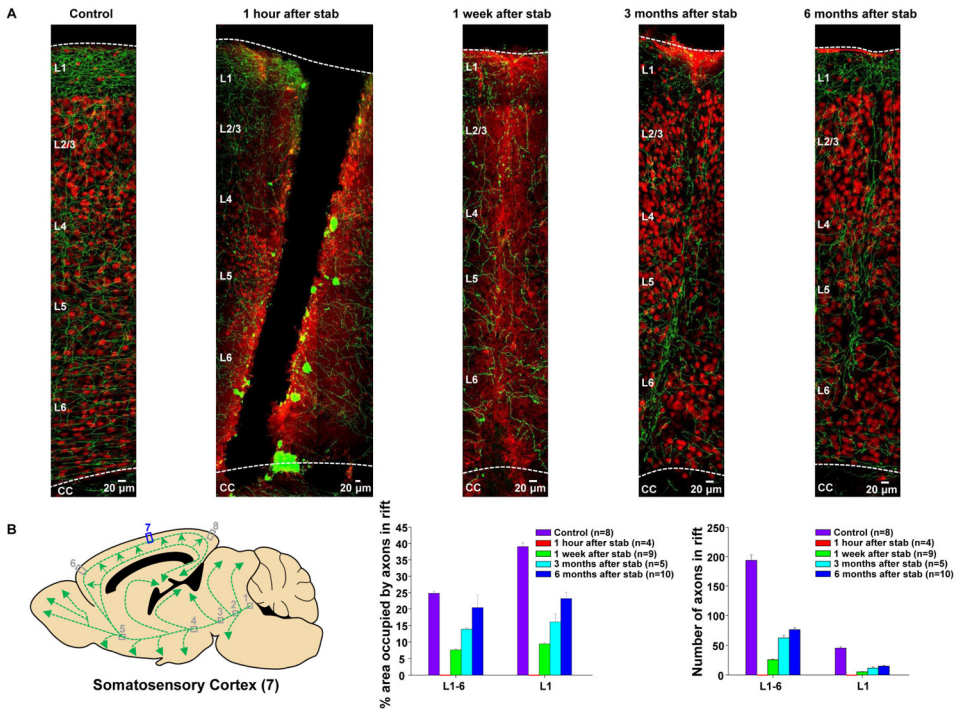

Figure 8. Serotonin axon regrowth in the adult mouse brain after stab injury as shown by immunohistochemistry

(**A**) In serotonin-transporter-EGFP mice, the serotonin axons were labeled with an antibody directed against GFP (green), and a subset of neurons were labeled with the nuclear marker NeuN (red) to provide landmarks. In stab-lesioned mice, serotonin axons were completely lost in the rift area at the 1 hour post-lesion time point and small number of axons started to enter the stab rift zone area 1 week after injury, becoming greater at later time points.

(**B**) The left panel shows a schematic representation of the serotonin neurons of the dorsal raphe and their C-shaped projection to the neocortex in the sagittal plane. The right panel shows the normalized area occupied by the serotonin-EGFP signal at various time points in stab injured and control mice within the rift zone in the somatosensory cortex (location 7).